Binding mechanism of arsenate on rutile (110) and (001) planes studied using grazing-incidence EXAFS measurement and DFT calculation

Meiyi Zhang, Guangzhi He, Gang Pan*

Department of Environmental Nano-materials, Research Center for Eco-Environmental Sciences,

Chinese Academy of Sciences, Beijing 100085, China

E-mail: myzhang@rcees.ac.cn, gzhhe@rcees.ac.cn, gpan@rcees.ac.cn

*Corresponding author. Phone: +86-10-62849686; Fax: +86-10-62849686; E-mail: gpan@rcees.ac.cn

Abstract: Characterization of contaminant molecules on different exposed crystal planes is required to conclusively describe its behavior on mineral surfaces. Here, the structural properties and relative stability of arsenate adsorbed on rutile TiO_2 (110) and (001) surfaces were investigated using grazing-incidence extended X-ray absorption fine structure (GI-EXAFS) spectra and periodic density functional theory (DFT) calculation. The combined results indicated that arsenate mainly formed inner-sphere bidentate binuclear (BB) and monodentate mononuclear (MM) complexes on both surfaces, but the orientational polar angles of arsenate on the (110) surface were commonly smaller than that on the (001) surface for the two adsorption modes. The DFT calculation showed that the (110) plane had a higher affinity toward arsenate than the (001) plane, suggesting that, for a given adsorption mode (i.e., MM or BB structure), a small polar angle was more favorable for arsenate stabilized on the rutile surfaces.

1. Introduction

Arsenic contamination in drinking water and groundwater resources has been a serious environmental problem due to its toxic impact on human health (Oremland and Stolz, 2003). Solid-water interfacial behaviors control arsenic mobility, toxicity and bioavailability (Liu and Aydil, 2009; Singer et al., 2013). It is therefore important to determine the adsorption geometries and bonding interactions that hold the arsenic species to the surface, which is directly related to the reversibility, lability and surface reactivity, and is essential to predict their fate in the environment (Makov and Payne, 1995).

Atomic-level understanding of the structure of contaminant molecules on mineral surfaces is growing through the application of spectroscopic and computational techniques, such as extended X-ray absorption fine structure (EXAFS) spectroscopy and density functional theory (DFT) calculation (Sherman and Randall, 2003; Zhang et al., 2005; He et al., 2009; Shimizu et al., 2011; Li et al., 2012). Over the last decades, EXAFS spectroscopy was successfully applied to determine the structure of adsorbates at water-mineral interfaces, and has been one of the most important techniques for structural analysis (Waychunas et al., 1993; Makov and Payne, 1995; Arai et al., 2001). However, standard EXAFS experiment are carried out using powder samples, where different types of crystal planes of the mineral are mixed. Multiple surface terminations and extensive defects of mineral powder produce a large number of different sites where adsorbates may adsorb (Catalano et al., 2005). Therefore, the structural data obtained from standard powder EXAFS spectra are therefore an average for various crystal planes.

These problems can be overcome by using grazing-incidence EXAFS (GI-EXAFS) spectroscopy. GI-EXAFS uses well-characterized single-crystal sample and polarized X-ray, which enables it to offer more structural information (interatomic distance, coordination number and polar angle) toward

3

the oriented absorbates than standard powder EXAFS (Waychunas et al., 2005). These advantages

may trigger wide applications of GI-EXAFS in geosciences, chemistry and environmental sciences as

synchrotron facilities are improving (Roscioni et al., 2013). Density functional theory (DFT)

calculation can provide a detailed description of adsorbed molecules at solid surfaces, including

aspects of structure, bonding, and energy (He et al., 2011; Li et al., 2012). Therefore, the combination

of GI-EXAFS and DFT calculation is able to identify the structural properties and relative stability of

arsenic on specific crystal planes.

Rutile, the most abundant polymorph of TiO_2, is one of the most common and technologically

important metal oxides for modern science and technology (Wang et al., 1997; Liu and Aydil, 2009),

and shows a high affinity to arsenic (Pena et al., 2005; Luo et al., 2010). The (110) surface is the

predominantly exposed plane of natural rutile (60%), and the (001) surface is studied intensively in

surface science due to its large-coordinate unsaturation (Ramamoorthy et al., 1994; Ahmed et al.,

2011).

Here we apply GI-EXAFS spectroscopy and periodic DFT calculation to study the binding

mechanism of arsenate on rutile (110) and (001) surfaces. In the GI-EXAFS measurement, two

directions of the X-ray electric vector, parallel and perpendicular to the substrate, were used to

determine the structure of the adsorbed arsenate on both surfaces. Periodic DFT calculation was

carried out to describe the bonding and energetic properties of arsenate on rutile TiO_2 surfaces.

2. Experimental and theoretical methods

### 2.1. Sample preparation

Highly polished $10\times10\times0.5$ mm^3 rutile TiO_2 (110) and (001) single crystals were obtained

commercially from Shanghai Daheng Optics and Fine Mechanics Co., Ltd, China. The orientations were

checked using high accuracy X-ray single crystal orientation instrument (DX-4A, Dandong, China) and

were found to be perfectly oriented to the resolution limits of the equipment (~2 Å). The roughness was

assessed with AFM (Veeco Dimension 3100) and was found to be ≤5 Å rms. Prior to initial use, the

crystals were washed in 10^{-4} M nitric acid and ethanol followed by multiple rinses with MilliQ (18 MΩ)

water. The crystals were then equilibrated with 0.1 M Na_2HAsO_4 solution at pH 6.8 for 2h to achieve a

sufficient adsorption density and hence adequate signal-to-noise ratio for GI-EXAFS data collection. A

constant ionic strength was maintained by use of 0.01 M $NaNO_3$. All chemicals used for solution

preparation were of reagent grade quality.

2.2. GI-EXAFS data collection

Grazing-incidence EXAFS data were collected on beamline BL14W1 at the Shanghai Synchrotron

Radiation Facility (SSRF) using a purposely build apparatus (Fig. 1). The instrument consists of a

carriage that holds the sample stage (KOHZU multi-dimensional sample stage), with motor drives for

positioning the sample over 5 degrees of freedom (Waychunas et al., 2005). Then, a wet arsenate-loaded

crystal sample was prepared on the sample stage for GI-EXAFS measurements. The carriage can be

rotated around the incident X-ray beam to set the angle of the X-ray electric vector polarization plane

with respect to the sample surface. Ionization chamber detectors were mounted on both sides of the

sample for transmission absorption data collection, and a 4-channel Si drift detector (SDD, Canberra

Industries, Inc.) was used to collect fluorescence signals.

87
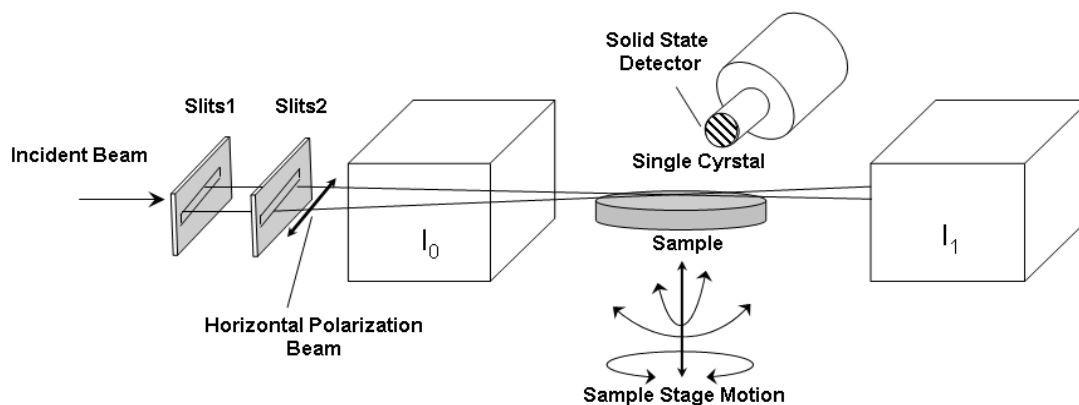
Fig. 1. Apparatus used in the GI-EXAFS data collection (SSRF, BL14W1). I_0 and I_1 are gas ionization

chambers for measuring the intensities of the incident beam and the reflected beam from the sample

surface, respectively.

The angle of the incident X-rays (beam diameter of ~30 μm) to the single-crystal surfaces was set to

0.15°, which is less than the critical angle of rutile TiO_2 at the energy position of As K-edge

(Klockenkämper, 1997). The experimental uncertainty on the incident angle of X-rays is $\leq 0.01°$. The

GI-EXAFS experiments were carried out using two scan modes with the electric vector parallel and

perpendicular to the single-crystal substrate. Samples were mounted in a Teflon cell and sealed with

Mylar film during the GI-EXAFS measurements. The cell was continuously purged with a constant

flow of water-saturated ultrapure N_2 to keep the crystals moist. An average of 3 scans was performed

to achieve suitable single/noise, and no obvious change in spectral data was observed during the 3

scans.

2.3. GI-EXAFS data analysis

The spectral data were processed following the standard procedures of background absorption

removal, normalization, k-space conversion, and Fourier transformation, and then the structural

information was extracted using WinXAS 3.1 software package with Fourier filtering and shell fitting

(Ressler, 1998). A linear function fit for the pre-edge region and a second-order polynomial fit in the

105 post-edge region were used to yield the normalized and background-corrected spectra. Subsequently,

106 the normalized spectra were converted to frequency (k) space using a cubic spline and weighted by k^3.

107 The $k^3\chi(k)$ spectra, from 2.2 to 12.0 Å^{-1}, were Fourier-transformed (FT) to R space using a Bessel

108 window function with smoothing parameter of 4. The theoretical phase shift and amplitude functions

109 for single- and multiple-scattering paths were calculated by ab initio Feff 9.0 code (Ankudinov et al.,

110 1998) using the cluster of scorodite (FeAsO$_4$·2H$_2$O) with the Fe atom replaced by Ti atom. This

111 method has been successfully used in the study of arsenate adsorption on Ti- and Al-(hydr)oxide

112 surfaces (Arai et al., 2001; Pena et al., 2006). An amplitude reduction factor (S_0^2) of 0.9 was used in

113 data-fitting procedure (Jing et al., 2005; Grafe et al., 2008). The coordination number (CN) of As-O

114 shell and two As-Ti subshells were initially fixed at 4, 2, and 1, respectively, to obtain estimated

115 values for interatomic distances (R), DW factors σ^2, and ΔE_0 (within ±6.0 eV). Then the R, σ^2, and ΔE_0

116 were fixed to obtain the estimated CN for each shell. The estimated values of CN, R, σ^2 and ΔE_0 were

117 then used for a sequential fitting that recorded the reduction of the residual until the best fit was

118 obtained. Finally, all the parameters (CN, R, σ^2 and ΔE_0) for each backscattering paths were allowed to

119 vary. All the residuals were less than 11%, indicating the good quality of the final data fitting. The

120 experimental spectra were also fitted using the As-As scattering path and As-O-O-As multiple

121 scattering path (see Supplementary data), and no significant improvement was found by adding the

122 As(V)-bearing solid phase and multiple scattering effects to the fitting.

123 *2.4. Computational settings*

124 All calculations were performed using the density functional theory (DFT) code DMol3 module in

125 Materials Studio software (Accerlys Software Inc.) under periodic boundary conditions (PBC) (Delley,

126 1995). In the spin-restricted DFT calculations, the exchange-correlation interaction was treated with the

127   generalized gradient approximation (GGA) parameterized by Perdew, Burke and Enzerhof (PBE)

128   (Perdew et al., 1996). A double numerical plus polarization (DNP) basis set (including a polarized

129   d-function for all non-hydrogen atoms and p-function for all hydrogen atoms) (Delley, 2000) and a

130   global orbital cutoff of 5.2 Å were employed. The size of the DNP basis set is comparable to Gaussian

131   6-31G (d, p), but the DNP is more accurate than a Gaussian basis set of the same size (Inada and Orita,

132   2008). The core electrons were treated with effective core potentials (ECP) (Hay and Wadt, 1985). The

133   conductor-like screening model (COSMO) was applied to simulate the water solvent environment

134   (Klamt and Schuurmann, 1993). The fine quality mesh size for the numerical integration was chosen.

135   The Brillouin zone was sampled using the Monkhorst-Pack special k-point scheme with a $4\times4\times1$ mesh

136   for structural optimization. To improve sampling convergence, a Fermi smearing of 0.005 hartree (1

137   hartree = 27.2114 eV = 2625.5 kJ mol^{-1}) was used (Delley, 1995). The geometry optimization

138   convergence tolerances of the energy, gradient, and displacement were 1×10^{-5} Hartree, 2×10^{-3} Hartree

139   Å^{-1}, and 5×10^{-3} Å, respectively.

140   *2.5. Computational model*

141   The unit cell of rutile TiO_2 was firstly optimized, and the obtained lattice constant (a = 4.646 Å, c =

142   2.988 Å) agreed favorably with the experimental values (a = 4.594 Å, c = 2.959 Å) (Baur and Khan,

143   1971) and other theoretical works (Perron et al., 2007). The supercell expansions and lattice

144   parameters used to construct each surface slab are listed in Table 1. The rutile (110) surface model

145   was constructed by a 2×1 surface supercell of 5.92 Å$\times$6.50 Å. The surface model consisted of four

146   O-Ti-O tri-layers (i.e., twelve atomic planes) with the thickness of 13.70 Å (Fig. 2a). During the DFT

147   calculations, the arsenate and the top two TiO_2 layers (i.e., six atomic planes) were allowed to relax,

148   and the bottom two TiO_2 layers were fixed at equilibrium crystal lattice sites to simulate bulk

149   conditions (Ojamäe et al., 2006; Huang et al., 2011). A 3D supercell consisted of 2×2 non-primitive

150   surface unit cells was created to model the (001) surface. Eight atomic planes were included in this

151   model, which resulted in the spatial dimensions of 9.19 Å×9.19 Å×11.84 Å (Fig. 2b). During the

152   geometrical optimization, the positions of arsenate and the top four atomic planes were allowed to

153   relax, and the bottom four atomic planes were fixed at the bulk crystal lattice sites. Hydroxylation of

154   rutile TiO_2 surfaces would occur in the solution, and the specific protonation states of the Ti-O is

155   controlled by pH. It has been determined that the protonation constants of rutile surfaces were 5.9 and

156   4.9 for the terminal (pK_{H1}, $TiOH^- + H^+ = TiOH_2$) and bridging (pK_{H2}, $Ti_2O^- + H^+ = Ti_2OH$) oxygen

157   sites, respectively (Machesky et al., 2008). According to the protonation constants, the $TiOH^-$

158   (terminal sites) and Ti_2O^- (bridging sites) groups should be the dominant species on rutile surfaces

159   under the GI-EXAFS experimental pH 6.8 condition. Therefore, the rutile surfaces were terminated by

160   protonated terminal oxygens and unprotonated bridging oxygens in the calculation of arsenate surface

161   complexation (see Fig. 2 and 4), corresponding to the pH condition in our GI-EXAFS experiment.

162   These models were separated from their periodic images normal to the surface by a vacuum gap of 15

163   Å to eliminate spurious interactions between the adsorbate and the periodic image of the bottom layer

164   of the slabs (Huang et al., 2011; Roscioni et al., 2013). A counter positive charge was automatically

165   added by DMol3 package during the calculations in order to keep the neutrality of the whole model to

166   avoid divergence in the electrostatic energy (Makov and Payne, 1995).
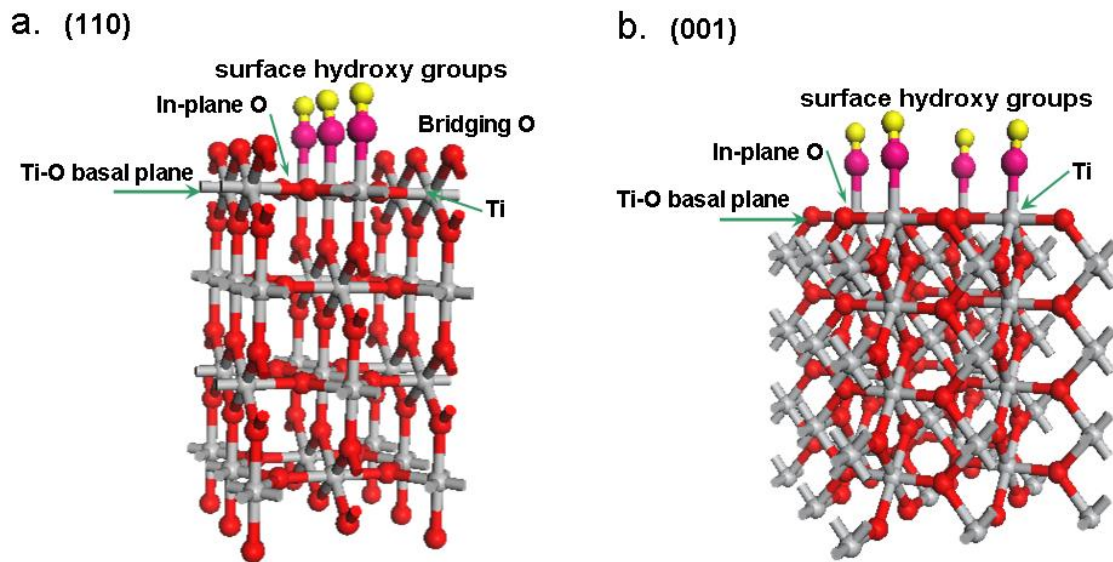
Fig. 2. Rutile TiO$_2$ (110) and (001) surface models used in the DFT calculation. Gray, red, big purple and yellow balls represent titanium, oxygen in rutile bulk, surface hydroxyl oxygen and hydrogen atoms, respectively.

Table 1. Supercell expansions and lattice parameters used to construct rutile (110) and (001) surface models

surface	expansion	U(Å)	v(Å)	area(Å^2)	n_{TiO_2}
(110)	2×1	5.98	6.57	38.45	30
(001)	2×2	9.29	9.29	84.42	42

The selection of parameters and models was justified by performing test calculations (see Table S1 and Fig. S4 in Supplementary data). Increasing k-points from 4×4×1 to 5×5×3 and orbital cutoff from 5.2 to 6.0 had almost no effect on adsorption geometry and energy. Similarly, no obvious difference was found in the adsorption structure when the relaxed O-Ti-O tri-layers increased from 2 to 3, and the corresponding change in binding energies was less than 4 kJ mol^{-1}. This result indicated that the structure and relative energy of arsenate adsorption were converged when the relaxed O-Ti-O tri-layers increased to 2, which were in line with the DFT results for other adsorbates in literatures (Ojamäe et al., 2006; Zhang et al., 2006; Huang et al., 2011). Addition of four explicit H$_2$O molecules to the model was

181   carried out to test the effects of outer-sphere H_2O molecules on the surface complexation of arsenate.

182   The results showed that the outer-sphere H_2O molecules do not strongly affect the geometry of adsorbed

183   arsenate (As-O distances shifted by <0.02 Å, As-Ti distances shifted by <0.01 Å, polar angles deviated

184   by less than 1°, and the difference in binding energies was less than 8 kJ/mol). These tests verified that

185   the present parameters and models were reliable for describing the properties of arsenate on rutile

186   surfaces.

3. Results and discussion

187

188   *3.1. GI-EXAFS analysis*

189   The k^3-weighted and Fourier transform spectra of As K-edge GI-EXAFS for the adsorption samples

190   of arsenate on rutile (110) and (001) single-crystal surfaces are shown in Fig. 3. The fitting data are

191   presented in Table 2. Based on our fitting results, we estimated the accuracies of the As–O shell to be

192   ±0.005 Å for interatomic distance (R) and ±5% for coordination number (CN_{As-O}). The estimated

193   errors were ±0.02 Å, ±0.03 Å and ±20% for R of As–Ti first subshell, R of As–Ti second subshell and

194   CN_{As-Ti}, respectively. The fitting results showed that the first coordination shell of the arsenic atom

195   consisted of four oxygen atoms at a distance of ~1.71 Å, which agreed with the literature (Pena et al.,

196   2006). As a result of the high symmetry of AsO_4 tetrahedron ($H_2AsO_4^-$ belongs to C_{2v} point-group

197   symmetry), no obvious difference in CN_{As-O} (Table 2) was observed between both polarized scans

198   (electric vector parallel and perpendicular to the substrate).

199   GI-EXAFS fitting results showed that the second peak (at 2.3-3.4 Å) of the Fourier transform

200   spectra was dominated by two titanium subshells (Table 2). The experimentally measured As-Ti

201   distances [3.27±0.02 Å and 3.58±0.03 Å on (110) plane, 3.31±0.02 Å and 3.56±0.03 Å on (001) plane]

11

202 were consistent with the DFT calculated values of bidentate binuclear (BB) [3.26 Å for (110) surface,

203 3.36 Å for (001) surface] and monodentate mononuclear (MM) [3.63 Å for (110) surface, 3.60 Å for

204 (001) surface] complexes, respectively (see Table 3). The As-Ti shells were also fitted using one

205 single As-Ti scattering path. The residuals of single-shell fits were commonly larger than that of

206 two-subshell fits (see Supplementary data), which confirmed the multiple coordination structures (i.e.,

207 the mixture of BB and MM adsorption) of arsenate on rutile surfaces.
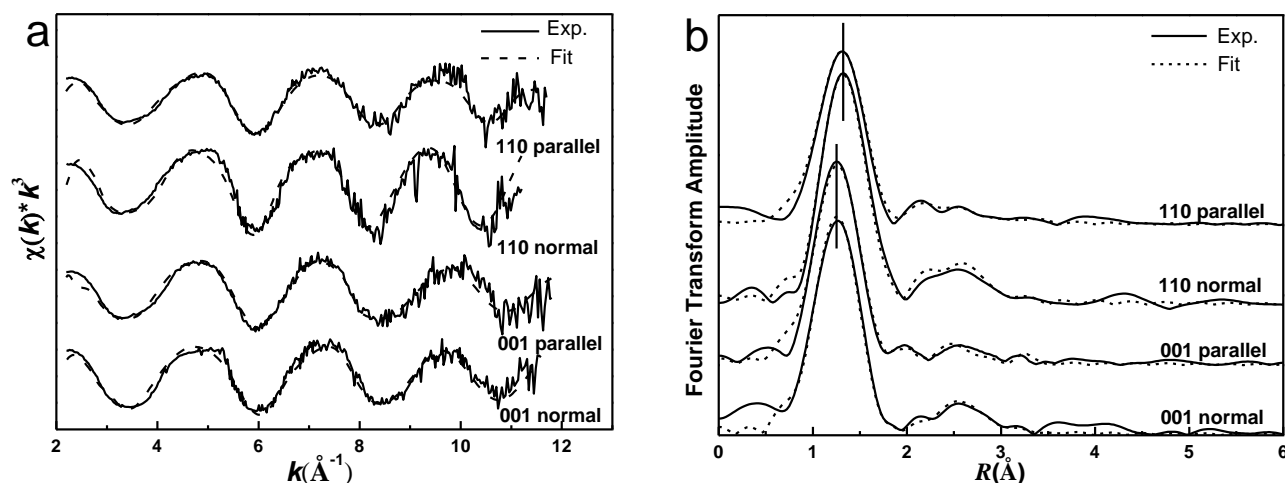
208

209 **Fig. 3.** (a) k^3-weighted and (b) Fourier transform As K-edge GI-EXAFS spectra of arsenate adsorption

210 on rutile (110) and (001) planes measured using two scan modes (electric vector parallel and

211 perpendicular to the substrate). The solid lines are the experimental spectra, while the dashed lines are

212 fitting curves. The peak positions are uncorrected for phase shifts.

213 An obvious difference in CN_{As-Ti} was observed from the same sample between the two scan

214 modes (Table 2), resulting from the polarization dependence of As-Ti bonds. Different to the CN_{iso}

215 determined by standard powder EXAFS, the polarized coordination number (CN_{pol}) obtained from

216 GI-EXAFS varies with the angle between the incident electric vector and the bond (Waychunas et al.,

217 2005). The polarization dependence allows a maximum of CN_{pol} when the bond parallel to the

12

218 direction of electric vector, and a near-zero value would appear when the bond normal to the electric

219 vector in the GI-EXAFS measurement. For instance, Fitts *et al.* presented that the CN_{pol} of Cu-Si bond

220 on SiO$_2$ (0001) surface in monodentate complex was 0.3 when the electric vector parallel to the

221 substrate (Fitts et al., 1999). It was also reported that a zero CN_{pol} value of Co-O bond occurred in an

222 on-top complex of Co(II) adsorbed on α-Al$_2$O$_3$ (0001) surface when the bond was absolutely normal

223 to the E-vector (Shirai et al., 1992; Shirai et al., 1994). The difference of CN_{As-Ti} between both

224 polarized scans can be used to deduce the polar angle (ϕ, angle between the As-Ti vector and the

225 substrate normal), and to determine the stereostructure of each surface complex. For the two scan

226 modes (electric vector parallel and perpendicular to the support plane), the relationships between the

227 coordination numbers of a polarized EXAFS measurement (CN_{pol}) and that of isotropic EXAFS (CN_{iso})

228 are $CN_{pol}^{\perp} = CN_{iso} \times 3\cos^2\phi$ and $CN_{pol}^{\parallel} = \dfrac{3}{2}CN_{iso} \times \sin^2\phi$, respectively (Manceau et al., 2002;

229 Waychunas et al., 2005). Based on the two equations, the polar angles (ϕ) of BB complex obtained

230 from GI-EXAFS fitting were 31°±8° on (110) surface and 43°±5° on (001) surface, while the

231 experimental ϕ of MM complex on (110) and (001) surfaces were 15°±6° and 18°±9°, respectively.

232 **Table 2**. GI-EXAFS measured structural parameters of arsenate adsorption on rutile (110) and (001)

233 single-crystal planes[a]

Shell	R(Å)	CN_{pol}	Type of neighbor	DW(σ^2)	ΔE_0	Residual[c] (%)
(110) surface E-vector[b] parallel to surface						
First	1.73 ± 0.005	4.0 ± 0.2	O	0.004 ±0.002	-1.566 ± 0.161	
Second	3.27 ± 0.02	0.7 ± 0.1	Ti	0.006 ±0.003	3.621 ± 0.073	10.5
	3.57 ± 0.03	0.2 ± 0.1	Ti	0.007 ±0.002	4.814 ± 0.051	
(110) surface E-vector normal						
First	1.73 ± 0.005	4.0 ± 0.2	O	0.004 ±0.001	-1.429 ± 0.019	
Second	3.28 ± 0.02	4.4 ± 0.8	Ti	0.005 ±0.002	4.013 ±0.017	6.5
	3.59 ± 0.03	2.8 ± 0.6	Ti	0.007 ±0.003	-5.580 ± 0.012	

(001) surface E-vector parallel to surface						
First	1.70 ± 0.005	4.0 ± 0.2	O	0.005 ±0.002	0.541 ±0.015	
Second	3.30 ± 0.02	1.6 ± 0.3	Ti	0.008 ±0.002	-3.986 ±0.650	10.7
	3.55 ± 0.03	0.3 ± 0.1	Ti	0.007 ±0.003	-5.683 ± 1.107	
(001) surface E-vector normal						
First	1.70 ± 0.005	4.0 ± 0.2	O	0.003 ±0.001	-1.487 ±0.007	
Second	3.33 ± 0.02	3.2 ± 0.6	Ti	0.006 ±0.002	3.365 ±0.002	5.1
	3.56 ± 0.03	2.7 ± 0.5	Ti	0.006 ±0.003	5.705 ±0.009	

[a] The listed parameters (CN, coordination number; R, interatomic distance; σ^2, Debye-Waller factor) reflected the final best fit.

[b] E-vector, electric vector.

[c] Residual gives a measure of the agreement between experimental and theoretical FT curves. All Residuals are < 11%, indicating reliable fits.

3.2. Periodic DFT calculation

$H_2AsO_4^-$ is the predominant species of $H_nAsO_4^{3-n}$ (pKa$_1$=2.2, pKa$_2$=7.0) (Ladeira et al., 2001) under the GI-EXAFS experimental pH 6.8 condition, and hence was used in the DFT calculation as the arsenate species. Calculated structures of arsenate on rutile (110) and (001) surfaces are shown in Fig. 4. DFT results showed that the average As-O bond lengths of arsenate tetrahedron in different adsorption states were about 1.73 Å (Table 3), which were generally slightly longer than the experimentally measured As-O distances (1.70-1.73 Å). This phenomenon was also observed in the adsorption of arsenite on Fe-(hydr)oxides (Zhang et al., 2005). This difference between experimental and theoretical values may be due to the theoretical underestimation of solvent effect from COSMO model (Costentin et al., 2004; Tossell, 2005). However, we expect that this artifact does not affect the relative stability of the adsorption modes and their complexation properties. DFT-calculated polar angles (ϕ, angle between the As-Ti vector and the substrate normal) of the BB and MM complexes on the rutile (110) surface were 27° and 6°, respectively. On the rutile (001) surface, the calculated ϕ were respectively 42° and 19° for the BB and MM complexes (Table 3). The discrepancies between experimental and DFT-calculated polar angles were less than 10°, indicating that a good estimation of the polar angles

254   was obtained.

255   Bidentate mononuclear (BM) complex was the potential adsorption mode at the bridging oxygen sites

256   on (110) surface (see Fig. S4 in Supplementary data). Our DFT results indicated that BM adsorption

257   mode would yield an As-Ti distance of 2.88 Å, much smaller than the distance obtained from

258   experimental GI-EXAFS measurement (3.30 ± 0.02 Å and 3.57 ± 0.03 Å), which confirmed the fact that

259   the twofold bridging oxygen is less active than the high coordination-unsaturated terminal oxygen at the

260   rutile (110) surface (Ojamäe et al., 2006; Li et al., 2012). Our previous DFT study showed that the

261   forming of outer-sphere H-bonded complexes were more thermodynamically unfavorable than

262   inner-sphere adsorption of arsenate on anatase TiO_2 surfaces (He et al., 2009). Moreover, the As-Ti

263   distances would be ~5 Å in outer-sphere $Ti-AsO_4$ complexes, however, no effective signals were

264   observed more than 4 Å away from the As atom in the GI-EXAFS spectra (see Fig. 3b). Therefore, in

265   order to directly compare the calculated results with experimental data, complexation at the bridging

266   oxygen sites on (110) surface and outer-sphere adsorption was not included in the analysis and

267   discussion here.

268

a   **b**   **c**   **d**
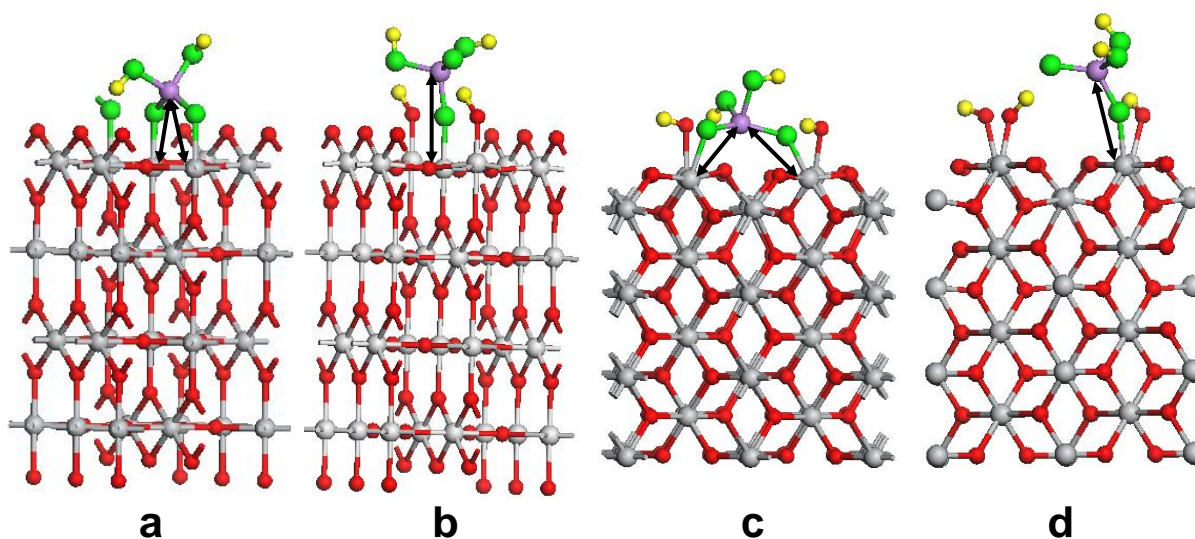
269 **Fig. 4.** DFT-calculated structures of arsenate adsorbed on rutile TiO_2 surfaces: (a) BB complex on

270 (110) plane; (b) MM complex on (110) plane; (c) BB complex on (001) plane; (d) MM complex on

271 (001) plane. Gray and red circles denote the Ti and O atoms in the TiO_2, respectively. Purple and

272 green circles denote As and O atoms in the AsO_4 tetrahedron, respectively. Yellow circles represent

273 the H atoms.

274 **Table 3.** DFT-calculated interatomic distances, polar angles and binding energies (ΔE) of arsenate

275 adsorbed on rutile surfaces

Bond	Interatomic distances (Å)							Polar angle (°)		Average	ΔE (kJ mol^{-1})
	As-O		As-OH		Average	As-Ti		Average			
BB-110	1.69	1.70	1.77	1.78	1.74	3.25	3.27	3.26	27	27	27	-261.4
MM-110	1.69	1.74	1.74	1.76	1.73	3.63		3.63	6	−	6	-265.9
BB-001	1.68	1.75	1.75	1.79	1.74	3.30	3.42	3.36	38	46	42	-245.5
MM-001	1.67	1.70	1.79	1.80	1.74	3.60		3.60	19	−	19	-161.4

276 Polar angle is the angle between the surface normal and the interatomic As-Ti vector direction.
277 ΔE were calculated as $\Delta E = E_{tot}(\text{Ti-AsO}_4)- [E_{tot}(\text{arsenate}) + E_{tot}(\text{TiO}_2)]$, where $E_{tot}(\text{Ti-AsO}_4)$ was the total energy of
278 Ti-AsO$_4$ adsorption complex, $E_{tot}(\text{arsenate})$ and $E_{tot}(\text{TiO}_2)$ were the total energy of arsenate molecule and TiO$_2$ cluster,
279 respectively. The structure of non-adsorbed arsenate were optimized in a periodic box with a side length of 10 Å
280 (Ojamäe et al., 2006).

281   Based on the spectral and computational results, the polar angles of monodentate and bidentate

282 complexes on the (110) surface were both smaller than that on the (001) surface (see Table 3).

283 DFT-calculated energies showed that adsorptions on the (110) plane (-261.4 kJ mol^{-1} for BB complex

284 and -265.9 kJ mol^{-1} for MM complex) were generally energetically more favorable than that on the (001)

285 plane (-245.5 kJ mol^{-1} for BB complex and -161.4 kJ mol^{-1} for MM complex), indicating that the (110)

286 plane had a higher affinity toward arsenate.

287 **4. Conclusions**

288   The spectral and computational results showed that arsenate primarily bonded as bidentate

289 binuclear (BB) and monodentate mononuclear (MM) inner sphere complexes on both (110) and (001)

16

290 surfaces of rutile TiO$_2$, but the spatial orientations of adsorbed arsenate were different on the two

291 crystal planes (i.e., crystal-face-dependent). The orientational polar angles on the (110) surface were

292 commonly smaller than that on the (001) surface for both monodentate and bidentate complexes. The

293 DFT calculation showed that the (110) plane displayed a higher affinity toward arsenate, suggesting

294 that, for a given adsorption mode (i.e., MM or BB structure), a small polar angle was more favorable

295 for arsenate stabilized on rutile surfaces.

Acknowledgements

Appendix A. Supplementary data

303 Details on EXAFS fitting based on different path functions/models, and discussion on the validation

304 of computational settings. Supplementary data associated with this article can be found in the online

305 version, at

References

307 Ahmed, A.Y., Kandiel, T.A., Oekermann, T., Bahnemann, D., 2011. Photocatalytic activities of

308 different well-defined single crystal TiO$_2$ surfaces: anatase versus rutile. J. Phys. Chem. Lett. 2,

309 2461-2465.

Ankudinov, A.L., Ravel, B., Rehr, J.J., Conradson, S.D., 1998. Real-space multiple-scattering calculation and interpretation of x-ray-absorption near-edge structure. Phys. Rev. B 58, 7565-7576.

Arai, Y., Elzinga, E.J., Sparks, D.L., 2001. X-ray absorption spectroscopic investigation of arsenite and arsenate adsorption at the aluminum oxide-water interface. J. Colloid Interface Sci. 235, 80-88.

Baur, W.H., Khan, A.A., 1971. Rutile-type compounds. IV. SiO_2, GeO_2 and a comparison with other rutile-type structures. Acta Crystallogr. B 27, 2133.

Catalano, J.G., Trainor, T.P., Eng, P.J., Waychunas, G.A., Brown Jr, G.E., 2005. CTR diffraction and grazing-incidence EXAFS study of U(VI) adsorption onto α-Al_2O_3 and α-Fe_2O_3 (1102) surfaces. Geochim. Cosmochim. Acta 69, 3555-3572.

Costentin, C., Robert, M., Saveant, J.M., 2004. Stepwise and concerted electron-transfer/bond breaking reactions. solvent control of the existence of unstable π ion radicals and of the activation barriers of their heterolytic cleavage. J. Am. Chem. Soc. 126, 16834-16840.

Delley, B., 1995. DMol, a standard tool for density functional calculations: review and advances. in: Seminario, J.M.P., P. (Ed.). Theor. Chem. Comput. Elsevier, pp. 221-254.

Delley, B., 2000. From molecules to solids with the DMol(3) approach. J. Chem. Phys. 113, 7756-7764.

Fitts, J.P., Trainor, T.P., Grolimund, D., Bargar, J.R., Parks, G.A., Brown, G.E., 1999. Grazing-incidence XAFS investigations of Cu(II) sorption products at α-Al_2O_3-water and α-SiO_2-water interfaces. J. Synchrot. Radiat. 6, 627-629.

Grafe, M., Tappero, R.V., Marcus, M.A., Sparks, D.L., 2008. Arsenic speciation in multiple metal

332   environments: I. Bulk-XAFS spectroscopy of model and mixed compounds. J. Colloid Interface

333   Sci. 320, 383-399.

334   Hay, P.J., Wadt, W.R., 1985. Abinitio effective core potentials for molecular calculations-potentials for

335   K to Au including the ourermost core orvitals. J. Chem. Phys. 82, 299-310.

336   He, G., Pan, G., Zhang, M., 2011. Studies on the reaction pathway of arsenate adsorption at water-TiO_2

337   interfaces using density functional theory. J. Colloid Interface Sci. 364, 476-481.

338   He, G., Zhang, M., Pan, G., 2009. Influence of pH on initial concentration effect of arsenate adsorption

339   on TiO_2 surfaces: thermodynamic, DFT, and EXAFS interpretations. J. Phys. Chem. C 113,

340   21679-21686.

341   Huang, W.F., Raghunath, P., Lin, M.C., 2011. Computational study on the reactions of H_2O_2 on TiO_2

342   anatase (101) and rutile (110) surfaces. J. Comput. Chem. 32, 1065-1081.

343   Inada, Y., Orita, H., 2008. Efficiency of numerical basis sets for predicting the binding energies of

344   hydrogen bonded complexes: Evidence of small basis set superposition error compared to

345   Gaussian basis sets. J. Comput. Chem. 29, 225-232.

346   Jing, C., Liu, S., Patel, M., Meng, X., 2005. Arsenic leachability in water treatment adsorbents.

347   Environ. Sci. Technol. 39, 5481-5487.

348   Klamt, A., Schuurmann, G., 1993. COSMO - a new approcch to dielectric screening in solvents with

349   explicit expressions for the screening energy and its gradient. J. Chem. Soc., Perkin Trans. 2,

350   799-805.

351   Klockenkämper, R., 1997. Total reflection X ray fluorescence analysis. Wiley, New York

352   Ladeira, A.C.Q., Ciminelli, V.S.T., Duarte, H.A., Alves, M.C.M., Ramos, A.Y., 2001. Mechanism of

353   anion retention from EXAFS and density functional calculations: Arsenic (V) adsorbed on

19

354   gibbsite. Geochim. Cosmochim. Acta 65, 1211-1217.

355 Li, S.C., Jacobson, P., Zhao, S.L., Gong, X.Q., Diebold, U., 2012. Trapping nitric oxide by surface

356   hydroxyls on rutile TiO_2 (110). J. Phys. Chem. C 116, 1887-1891.

357 Liu, B., Aydil, E.S., 2009. Growth of oriented single-crystalline rutile TiO_2 nanorods on transparent

358   conducting substrates for dye-sensitized solar cells. J. Am. Chem. Soc. 131, 3985-3990.

359 Luo, T., Cui, J., Hu, S., Huang, Y., Jing, C., 2010. Arsenic removal and recovery from copper smelting

360   wastewater using TiO_2. Environ. Sci. Technol. 44, 9094-9098.

361 Machesky, M.L., Predota, M., Wesolowski, D.J., Vlcek, L., Cummings, P.T., Rosenqvist, J., Ridley,

362   M.K., Kubicki, J.D., Bandura, A.V., Kumar, N., Sofo, J.O., 2008. Surface protonation at the rutile

363   (110) interface: explicit incorporation of solvation structure within the refined MUSIC model

364   framework. Langmuir 24, 12331-12339.

365 Makov, G., Payne, M.C., 1995. Periodic boundar conditions in *ab initio* calculations. Phys. Rev. B 51,

366   4014-4022.

367 Manceau, A., Lanson, B., Drits, V.A., 2002. Structure of heavy metal sorbed birnessite. Part III:

368   Results from powder and polarized extended X-ray absorption fine structure spectroscopy.

369   Geochim. Cosmochim. Acta 66, 2639-2663.

370 Ojamäe, L., Aulin, C., Pedersen, H., Käll, P.-O., 2006. IR and quantum-chemical studies of carboxylic

371   acid and glycine adsorption on rutile TiO_2 nanoparticles. J. Colloid Interface Sci. 296, 71-78.

372 Oremland, R.S., Stolz, J.F., 2003. The ecology of arsenic. Science 300, 939-944.

373 Pena, M., Meng, X.G., Korfiatis, G.P., Jing, C.Y., 2006. Adsorption mechanism of arsenic on

374   nanocrystalline titanium dioxide. Environ. Sci. Technol. 40, 1257-1262.

375 Pena, M.E., Korfiatis, G.P., Patel, M., Lippincott, L., Meng, X., 2005. Adsorption of As(V) and As(III)

20

376   by nanocrystalline titanium dioxide. Water Res. 39, 2327-2337.

377   Perdew, J.P., Burke, K., Ernzerhof, M., 1996. Generalized Gradient Approximation Made Simple.

378   Phys. Rev. Lett. 77, 3865-3868.

379   Perron, H., Domain, C., Roques, J., Drot, R., Simoni, E., Catalette, H., 2007. Optimisation of accurate

380   rutile TiO_2 (110), (100), (101) and (001) surface models from periodic DFT calculations.

381   Theoretical Chemistry Accounts: Theory, Computation, and Modeling (Theoretica Chimica Acta)

382   117, 565-574.

383   Ramamoorthy, M., Vanderbilt, D., Kingsmith, R.D., 1994. 1st-principles calculations of the energetics

384   of stoichiometric TiO_2 surfaces. Phys. Rev. B 49, 16721-16727.

385   Ressler, T., 1998. WinXAS: a program for X-ray absorption spectroscopy data analysis under

386   MS-Windows. J. Synchrot. Radiat. 5, 118-122.

387   Roscioni, O.M., Dyke, J.M., Evans, J., 2013. Structural characterization of supported

388       $Rh^I(CO)_2/\gamma$-Al_2O_3 catalysts by periodic DFT calculations. J. Phys. Chem. C 117, 19464-19470.

389   Sherman, D.M., Randall, S.R., 2003. Surface complexation of arsenic(V) to iron(III) (hydr)oxides:

390   structural mechanism from ab initio molecular geometries and EXAFS spectroscopy. Geochim.

391   Cosmochim. Acta 67, 4223-4230.

392   Shimizu, M., Arai, Y., Sparks, D.L., 2011. Multiscale Assessment of Methylarsenic Reactivity in Soil.

393   1. Sorption and Desorption on Soils. Environ. Sci. Technol. 45, 4293-4299.

394   Shirai, M., Asakura, K., Iwasawa, Y., 1992. Anisotropic Structure-Analysis for Cobalt Oxides on

395   α-Al_2O_3 (0001) by Polarized Total-Reflection Fluorescence Extended X-Ray Absorption

396   Fine-Structure. Catal. Lett. 15, 247-254.

397   Shirai, M., Inoue, T., Onishi, H., Asakura, K., Iwasawa, Y., 1994. Polarized Total-Reflection

398   Fluorescence Exafs Study of Anisotropic Structure-Analysis for Co Oxides on Alpha-Al_2O_3 (0001)

399   as Model Surfaces for Active Oxidation Catalysts. J. Catal. 145, 159-165.

400   Singer, D.M., Fox, P.M., Guo, H., Marcus, M.A., Davis, J.A., 2013. Sorption and redox reactions of

401   As(III) and As(V) within secondary mineral coatings on aquifer sediment grains. Environ. Sci.

402   Technol. 47, 11569-11576.

403   Tossell, J.A., 2005. Theoretical study on the dimerization of $Si(OH)_4$ in aqueous solution and its

404   dependence on temperature and dielectric constant. Geochim. Cosmochim. Acta 69, 283-291.

405   Wang, R., Hashimoto, K., Fujishima, A., Chikuni, M., Kojima, E., Kitamura, A., Shimohigoshi, M.,

406   Watanabe, T., 1997. Light-induced amphiphilic surfaces. Nature 388, 431-432.

407   Waychunas, G., Trainor, T., Eng, P., Catalano, J., Brown, G., Davis, J., Rogers, J., Bargar, J., 2005.

408   Surface complexation studied via combined grazing-incidence EXAFS and surface diffraction:

409   arsenate an hematite (0001) and (1012). Anal. Bioanal. Chem. 383, 12-27.

410   Waychunas, G.A., Rea, B.A., Fuller, C.C., Davis, J.A., 1993. Surface-chemistry of Ferrihydrite .1.

411   EXAFS studies of the geometry of coprecipitated and adsorbed arsenate. Geochim. Cosmochim.

412   Acta 57, 2251-2269.

413   Zhang, N.L., Blowers, P., Farrell, J., 2005. Evaluation of density functional theory methods for

414   studying chemisorption of arsenite on ferric hydroxides. Environ. Sci. Technol. 39, 4816-4822.

415   Zhang, Z., Fenter, P., Kelly, S.D., Catalano, J.G., Bandura, A.V., Kubicki, J.D., Sofo, J.O., Wesolowski,

416   D.J., Machesky, M.L., Sturchio, N.C., Bedzyk, M.J., 2006. Structure of hydrated Zn^{2+} at the rutile

417   TiO_2 (110)-aqueous solution interface: Comparison of X-ray standing wave, X-ray absorption

418   spectroscopy, and density functional theory results. Geochim. Cosmochim. Acta 70, 4039-4056.

419